Since January 2020 Elsevier has created a COVID-19 resource centre with free information in English and Mandarin on the novel coronavirus COVID-19. The COVID-19 resource centre is hosted on Elsevier Connect, the company's public news and information website.

International Dairy Journal 137 (2023) 105488

Contents lists available at ScienceDirect

International Dairy Journal

journal homepage: www.elsevier.com/locate/idairyj

Hydrolysis improves the inhibition efficacy of bovine lactoferrin against infection by SARS-CoV-2 pseudovirus

Devashree Patil [a], Siyu Chen [a], Vincenzo Fogliano [a], Ashkan Madadlou [b,*]

[a] Food Quality and Design Group, Department of Agrotechnology and Food Sciences, Wageningen University and Research, Wageningen, the Netherlands
[b] Department of Biotechnology and Food Science, Norwegian University of Science and Technology (NTNU), Trondheim, Norway

ARTICLE INFO

Article history:
Received 1 August 2022
Received in revised form
26 August 2022
Accepted 27 August 2022
Available online 5 September 2022

ABSTRACT

The entry of SARS-CoV-2 into host cells may involve the spike protein cleavage by cathepsin L (CTSL). Certain food proteins such as lactoferrin (Lf) inhibit CTSL. The current study investigated the impact of hydrolysis (0–180 min) by proteinase K on electrophoretic pattern, secondary structure, cathepsin inhibitory and SARS-CoV-2 pseudovirus infectivity inhibitory of bovine Lf. Gel electrophoresis indicated that hydrolysis cut Lf molecules to half lobes (~40 kDa) and produced peptides ≤18 kDa. Approximation of the secondary structural features through analysis of the second-derivative amide I band collected by infra-red spectroscopy suggested a correlative–causative relationship between cathepsin inhibition and the content of helix-unordered structures in Lf hydrolysate. The half maximal inhibitory concentration (IC_{50}) of Lf hydrolysed for 90 min (H90) against CTSL was about 100 times smaller than that of the Lf hydrolysed for 0 min (H0). H90 had also double activity against SARS-CoV-2 pseudo-types infectivity compared with H0.

1. Introduction

The coronavirus 2019 (COVID-19) pandemic, caused by the severe acute respiratory syndrome coronavirus-2 (SARS-CoV-2) has posed unprecedented health challenges. Coronaviruses (CoVs) are enveloped positive-sense RNA viruses that bind to the human angiotensin-converting enzyme 2 (hACE2), found on the host cell membrane, via their spike glycoproteins (S proteins) (V'kovski, Kratzel, Steiner, Stalder, & Thiel, 2021). SARS-CoV-2 possesses modified S proteins and has a ten-to twenty-fold higher affinity for hACE2 receptors than the SARS-CoV (Xia et al., 2020), resulting in a faster transmission rate. The S protein is composed of two subunits: (a) S1 subunit – containing a receptor-binding domain (RBD) responsible for virus attachment to the ACE2 receptor (Xia et al., 2020); and (b) S2 subunit – containing a fusion peptide responsible for endocytosis (Hoffmann et al., 2020). The entry of SARS-CoV-2 into host cells takes place by two mechanisms: (a) membrane fusion in which transmembrane protease serine 2 (TMPRSS2) primes the S protein and (b) endocytosis where cathepsin L (CTSL), and phosphatidylinositol 3-phosphate 5-kinase are critical (Hoffmann et al., 2020; Ou et al., 2020; Zhao et al., 2021).

CTSL, a cysteine protease found in all tissues and cell types, is a matrix-degrading enzyme. Its principal function is proteolysis of protein antigens generated during pathogen endocytosis (Gomes et al., 2020; Liu et al., 2018). However, the excessive secretion of cysteine cathepsins is associated with a variety of pathological states in humans such as inflammation, apoptosis, tumour cell proliferation, and osteogenesis (Dana & Pathak, 2020; Fonović & Turk, 2014). Since inhibition of cathepsins can lead to the failure reversal (Mittal, Mir, & Chauhan, 2011), cathepsin inhibitory techniques and substances are enthusiastically pursued by researchers. Some studies suggested that CTSL inhibition may be a way to prevent SARS-CoV-2 infection in humans (Liu, Luo, Libby, & Shi, 2020; Ou et al., 2021; Zhao et al., 2021). In this context, synthetic cathepsin inhibitory drugs such as hydroxychloroquine and chloroquine were shown to interfere with the SARS-CoV-2 infection in human cells (Hoffmann et al., 2020; Ou et al., 2021).

Even though the above-mentioned in vitro evidence was not confirmed in human studies (Deng et al., 2022; Hernandez, Roman, Pasupuleti, Barboza, & White, 2020) the mechanistic pathway is worth investigating considering that some plant and animal foods contain cathepsin inhibitory compounds. Examples of the plant-based cathepsin inhibitors are bromelain inhibitor VI, and oryzacystain derived respectively from pineapple stem and rice. They share similar structural features such as (extensive) disulfide

* Corresponding author.
E-mail address: ashkan.madadlou@ntnu.no (A. Madadlou).

https://doi.org/10.1016/j.idairyj.2022.105488

crosslinks and absence or low contents of α-helix structures (Madadlou, 2020). Mammalian milk has also significant levels of cysteine protease inhibitors, the most important one is lactoferrin (Lf) (Ohashi et al., 2003).

Bovine Lf is a 78 kDa glycoprotein with an isoelectric point between pH 8 and 9. Lf is rich in cysteine and comprises two highly homologous lobes, representing the N-terminal and C-terminal halves of the polypeptide chain. Each lobe contains an iron-binding site (Moore, Anderson, Groom, Haridas, & Baker, 1997). Apparently, the iron-binding property have no effect on Lf antiviral activity (Wotring, Fursmidt, Ward, & Sexton, 2022). Lf was shown to inhibit SARS-CoV endocytosis by interacting with cell-surface heparan sulphate proteoglycans and thereby blocking the binding of S protein to HEK293E/ACE2-Myc cells (Lang et al., 2011). Lf may also suppress some viral infections by inhibiting cathepsins. While a synthetic peptide targeting the active site of CTSL had a half maximal inhibitory concentration (IC_{50}) of 10^{-5} M, Lf isolated from bovine and/or human milk had an IC_{50} value of approximately 10^{-6} M against CTSL (Sano et al., 2005). It is reported in the literature that bovine Lf inhibits the cysteine proteases in the following order: CTSL > papain > cathepsin S, with almost no inhibition of cathepsin B and H (Sano et al., 2005). The administration of Lf in the form of a liposomal bovine lactoferrin syrup was examined in treatment of COVID-19 patients, as well as the family members in contact with them. The treatment caused a complete and fast recovery in the patients, and prevented the illness in people directly in contact with the patients (Serrano et al., 2020).

Lf-derived peptides might show a higher antiviral activity than the parent protein. Recently, a well-known proteolytic product of Lf, i.e., lactoferricin was assessed for its antiviral activity against several of the new SARS-CoV-2 variants. The assessment indicated that the anti-SARS-CoV-2 activity of the peptide lactoferricin may add to the clinical significance of Lf for SARS-CoV-2 treatment (Wotring et al., 2022). Based on the results of a molecular docking early assessment which revealed that only the C-terminal lobe of Lf interacts with CTSL (Madadlou, 2020), it was hypothesised that cutting bovine Lf molecules to the half-molecules may be advantageous for CTSL inhibition. Either of the enzymes pepsin, trypsin or proteinase K can be used to generate peptide fragments of half the molecular mass of Lf (Sharma, Singh, & Bhatia, 1999; Singh et al., 2021). The objective of the current research was to hydrolyse bovine Lf by proteinase K and assess the inhibitory effect of the bovine Lf hydrolysate on the human cathepsins L, B, H, and K. Next, SARS-CoV-2 pseudovirus model tests were performed to determine whether the CTSL-inhibitory bovine Lf hydrolysate could prevent the infection of human cells under in vitro conditions.

2. Material and methods

2.1. Materials

High purity bovine Lf powder (with 95.9% protein comprising 96.4% Lf) was kindly provided by FrieslandCampina Ingredients (The Netherlands). Proteinase K, pefabloc SC, and 8-anilino-1-naphtalenesulfonic acid (ANSA) were purchased from Sigma–Aldrich (The Netherlands). 4–12% bis-Tris precast polyacrylamide gels, lithium dodecyl sulphate (LSD) sample buffer, Coomassie brilliant blue R250, sample reducing agent, antioxidant, and Spectra™ multicolour broad range protein ladder were purchased from Thermo Fisher Scientific (USA). For cathepsin inhibitory, cathepsin L, B, H, and K inhibitor screening kits (abcam.com) were used. All other chemicals used were of analytical grade unless otherwise stated, and the water used in the experiments was deionised water.

Serum from the National Institute for Biological Standards and Control (NIBSC, Herts, UK) with known neutralisation titre (Research reagent for anti-SARS-CoV-2 Ab NIBSC code 20/130) was used in pseudo-type viral infectivity assay (Hyseni et al., 2020). Moreover, negative serum, SARS-CoV-2 pseudo-types (full-length S-protein), and HEK 293 T/17 cells (human embryonic kidney 293 cells) (ATCC-CRL 1573) were used in the viral infectivity assay. HEK 293 T/17 cells were cultured in Dulbecco's Modified Eagle's Medium (DMEM) in high glucose (Euroclone, Pero, Italy) supplemented with 2 mM L-glutamine (Lonza, Milan, Italy), 100 units mL^{-1} penicillin-streptomycin (Lonza, Milan, Italy), and 10% feta (Euroclone, Pero, Italy) (Hyseni et al., 2020).

2.2. Hydrolysis of Lf

A buffer solution of 100 mM ammonium bicarbonate (NH_4HCO_3) in deionised water was prepared and pH was adjusted to 7.00 ± 0.02 using 0.5 M NaOH. A 0.2 mM solution of Lf in buffer was prepared and the pH was adjusted to 10 ± 0.02, followed by 5 min of slowly shaking at 20 °C. The solution was kept stored for 24 h at 4 °C to warrant complete hydration. Proteinase K and pefabloc SC solutions were prepared in 100 mM NH_4HCO_3 buffer (pH 7 ± 0.02) at concentrations of 1 mM and 200 mM, respectively. The Lf solution was incubated with proteinase K at 37 °C in a shaking water bath and the enzyme to Lf mass ratio was kept at 1:100 (Sharma et al., 1999). The hydrolysis pattern was observed at incubation times of 0, 30, 60, 90, 120, and 180 min. Immediately after hydrolysis, samples were cooled to room temperature (20 °C) within an ice bath, and supplemented with pefabloc SC at a pefabloc-to-Lf hydrolysate ratio of 1:50 (for proteinase K inactivation), followed by manual shaking for uniform mixing. The hydrolysates were kept at 20 °C for 5–10 min and stored at −20 °C until further analysis.

2.3. Gel electrophoresis

Sodium dodecyl sulphate-polyacrylamide gel electrophoresis (SDS-PAGE) analysis of Lf hydrolysate was performed under non-reducing and reducing conditions. The hydrolysate was diluted threefold to a concentration of 0.07 mM, uniformly mixed with a mixture of SDS-PAGE sample buffer (ratio 2:5, v/v) and treated with either 100 mM ammonium bicarbonate buffer (pH 10 ± 0.01, for non-reducing conditions) or dithiothreitol (for reducing conditions), followed by centrifugation for 1 min at 800×*g*. The samples were heated in a shaking water bath for 10 min at 70 °C and centrifuged for 1 min at 800×*g*. Aliquots (20 μL) of samples were loaded on 4–12% bis-Tris precast polyacrylamide gels, and Spectra™ multicolour broad range protein ladder was used as the molecular mass marker. After electrolysis, gels were rinsed with distilled water and stained with Coomassie brilliant blue R-250 for 3 h at 20 °C.

2.4. Cathepsin inhibitory assay

The activity of human cathepsins L, B, H, and K as influenced by the Lf hydrolysate was measured using fluorometric inhibitor screening kits. The assay uses the ability of active human cathepsin to cleave a synthetic substrate 7-amino-4-trifluoromethylcoumarin (AFC) and release a fluorescent component that could be detected and measured using a fluorescence microplate reader. Cleavage of substrate is decreased in the presence of a cathepsin inhibitor, resulting in reduced or no formation of AFC fluorescence. All cathepsin assays were performed in accordance with the detailed protocols outlined in the Abcam booklet (www.abcam.com).

For measuring the inhibitory efficacy on CTLS, a CTSL reagent aliquot was made by mixing 5 μL dithiothreitol (DTT) with CTSL

reagent. According to the preliminary experiments, the inhibitor compound was prepared by dissolving Lf hydrolysate (0–180 min hydrolysis time in replicates) in CTSL assay buffer at final concentrations of 1.45×10^{-8}, 6.25×10^{-7}, 2.50×10^{-6}, 7.50×10^{-5}, and 2.50×10^{-4} M. For measuring the inhibitory efficacy on other cathepsins (B, H, and K), a slightly different protocol was applied, i.e., DTT was not used. The difference in protocol was according to the manufacture (Abcam) guidelines. The wavelengths required to detect the activity of cathepsins B, H, and K [excitation/emission wavelengths ($\lambda_{Ex}/\lambda_{Em}$) = 400/505 nm] were also slightly different from those needed for cathepsin L ($\lambda_{Ex}/\lambda_{Em}$ = 405/505 nm). The duration of reading for cathepsin L was 30 min, while that for cathepsin B, H, and K was 120 min.

The activities of all cathepsins were monitored every 3 min in VersaMax microplate reader (Company: VersaMax™, Software: SoftMax Pro, Wageningen, the Netherlands) at 37 °C at previously stated fluorescence intensities (I) in a kinetic mode. The samples were measured in triplicates to account for standard errors. Irreversible inhibitors that fully inhibit cathepsin activity at the tested concentration had a relative fluorescence unit (RFU) = 0, and the percent relative inhibition was 100%.

2.5. Fourier-transform infra-red spectroscopy

For spectra acquisition, the FTIR measurements were taken with a Bruker Invenio-S FTIR spectrometer (Bruker Optik GmbH, Germany) and data acquisition was controlled by OPUS 8.5 software. The spectra were recorded in transmission mode from 4000 cm^{-1} to 400 cm^{-1} with a resolution of 4 cm^{-1}, an aperture of 6.0 mm, and a total of 60 scans. The background and buffer were collected before each sample scanning and subtracted at the same time, while 1% SDS and Milli-Q water were used to clean the cell.

For spectra analysis, the spectra were smoothed and normalised, and second-derivative spectra were obtained by Savitsky-Golay derivative method for a nine data point window using OPUS 8.5 software. Then the second derivative curves were cut from 1700 cm^{-1}–1600 cm^{-1} (amide I) and analysed by fitting Gaussian curve using OriginPro 2021 software (OriginLab Cooperation, Northampton, US). The quantification of secondary structures was performed by calculating each peak area as a percentage of the sum of all peak areas.

2.6. SARS-CoV-2 pseudo-type infectivity assay

2.6.1. Production of SARS-CoV-2 pseudo-types

The protocol described by Hyseni et al. (2020) was used to generate lentiviral-based pseudo-types containing the surface (S) glycoprotein of wild-type SARS-CoV-2 virus.

2.6.2. SARS-CoV-2 pseudo-type-based neutralisation assay

The bovine Lf hydrolysate samples were evaluated for their efficacy to neutralise the SARS-CoV-2 pseudovirus internalisation into HEK 293 T/17 cells (human embryonic kidney 293 cells). A control positive with 100% neutralisation activity (NIBSC serum, code 20/130) and a control negative serum with 0% neutralisation activity (Hyseni et al., 2020) were used in the assay. In brief, a two-fold serial dilution of samples, starting form 1:5 was performed in a culture medium [Dulbecco modified Eagle's medium (DMEM), 5% FBS, 1% penicillin-streptomycin (PEN-STREP), 1% L-glutamine]. In a 96-well culture plate, serum was combined with SARS-CoV-2 pseudo-types in a 1:1 v/v ratio. The virus input was 1×10^6 relative light units (RLU) $well^{-1}$. The HEK 293/ACE2 transfected cells (2.0×10^5 cell mL^{-1}) were seeded into each well of flat-bottomed tissue plates containing Lf hydrolysate and pseudo-type mixer and immediately incubated for 1 h at 37 °C in a humidified atmosphere with 5% CO_2. The plates were incubated for 48–72 h at 37 °C, and neutralising antibodies were detected using luciferase activity. Neutralising antibody titres were identified based on luciferase activity as endpoint of two-fold diluted test samples and the serum dilution that caused a 50% reduction of a single round of infection (reporter gene-mediated signal) was extrapolated. Then, the half maximal inhibitory concentration (IC_{50} titre) was calculated using the initial concentration of the titres (Hyseni et al., 2020).

2.7. Statistical analysis

All experiments were performed in duplicates with three measurements otherwise stated, and values were expressed as mean values ± standard deviation. For cathepsin inhibitor screening and SARS CoV-2 pseudo-type infectivity assays, IC_{50} values were determined using GraphPad Prism version 8.4 software. The titre readings were expressed as the dilution range within which the IC_{50} values fall (Hyseni et al., 2020). For all experiments, the differences between samples were assessed using one-way ANOVA at $p < 0.05$ significant level.

3. Results and discussion

3.1. Electrophoretic analysis of the Lf hydrolysate

Fig. 1 shows the SDS-PAGE profiles of the bovine Lf hydrolysate samples under non-reducing and reducing conditions. The not hydrolysed sample (i.e., hydrolysed for 0 min, H0) showed a major band at ~80 kDa under both conditions. The band corresponds to intact Lf. Also, a thin band at around 200 kDa was observed and attributed to protein aggregates (Goulding, O'Regan, Bovetto, O'Brien, & O'Mahony, 2021). Moreover, under the non-reducing condition, several thin bands between 22 and 58 kDa were observed (Fig. 1a). These bands are likely minor amounts of other milk proteins co-purified with Lf (Lönnerdal, Du, & Jiang, 2021) and/or large peptide fragments that were generated promptly by proteinase K despite its immediate inhibition after addition to the Lf solution.

Non-reducing SDS-PAGE indicated that hydrolysis significantly influenced the electrophoretic pattern of Lf. As a consequence of hydrolysis even for the shortest time, i.e., 30 min, the band at ~80 kDa almost completely disappeared (Fig. 1a) and two bands at 38 kDa and 43 kDa emerged. The band at 38 kDa was comparatively thicker than that at 43 kDa. The former probably corresponds to apo-Lf half molecule, whereas the latter was most likely monoferric Lf half molecule (Sharma et al., 1999). According to the manufacturer, the Lf preparation used in the current study had an iron saturation level of only 10% and, hence, generation of a thicker band for apo-Lf half-molecule was expected. The production of Lf half molecules due to hydrolysis confirms that proteinase K cuts Lf at the helix that covalently connects two lobes of Lf (Singh, Sharma, Karthikeyan, Betzel, & Bhatia, 1998). The peptide bond Arg341–Tyr342, which is a part of the inter-lobe 10-residue long helical peptide Thr334-Thr343 is cleaved by proteinase K (Singh et al., 2021). Under non-reducing SDS-PAGE, several bands at ≤18 kDa were observed in all the hydrolysate samples (≥30 min). These bands were not present in the non-hydrolysed sample (i.e., hydrolysed for 0 min, H0) (Fig. 1a). The small fragments (≤18 kDa) were most probably the hydrolysis products of the N-lobe and the C-lobe supposedly remained fully functional (Singh et al., 2021). The band at ~12 kDa became faint by hydrolysis ≥60 min.

Under the reducing SDS-PAGE the bands corresponding to Lf half molecule (38 kDa and 43 KDa) and the peptides of 18–22 kDa were not observed in the hydrolysate samples. However, SDS-PAGE

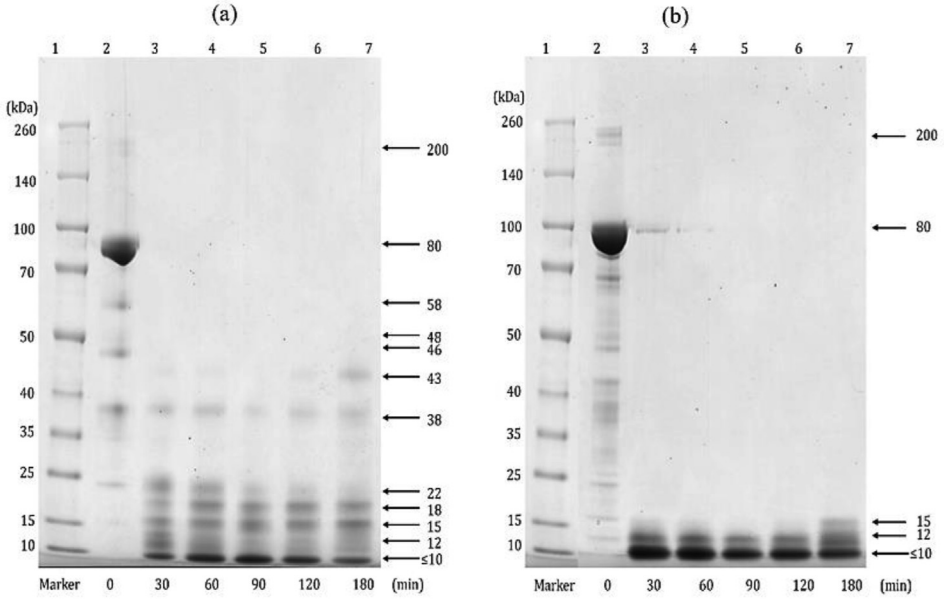

Fig. 1. SDS-PAGE gels of Lf hydrolysate under (a) non-reducing and (b) reducing conditions: lane 1, broad range protein marker; lanes 2–7, hydrolysis for 0, 30, 60, 90, 120, and 180 min, respectively.

bands corresponding to peptides with molecular masses below 15 kDa were observed under reducing condition (Fig. 1b). In agreement with our observation on Lf half molecules, Sharma et al. (1999) did not detect the band corresponding to Lf half molecules (~40 kDa) under reducing SDS-PAGE when they run hydrolysis of (buffalo) Lf at a high proteinase K-to-substrate ratio. However, when they applied an enzyme-to-substrate ratio comparable with the present study, smaller peptides (≤15 kDa) were not detected and only bands corresponding to Lf half molecules (~40 kDa) were detected under reducing SDS-PAGE (Sharma et al., 1999). The discrepancy between the results of our study and those of Sharma et al. (1999) is attributed to dissimilarities in the iron saturation level of the Lfs used in the two studies. The iron saturation level of the Lf used in the present study was 10%, whereas that of the Lf used by Sharma et al. (1999) was 80%. It is known that iron binding increases the molecular stability of Lf (Baker & Baker, 2004) and hence, iron-depleted (apo-lactoferrin) Lf has a looser structure than iron-saturated (holo-lactoferrin) Lf, causing differences in their proteolytic degradability (Bokkhim, Tran, Bansal, Grøndahl, & Bhandari, 2014).

3.2. Cathepsin inhibitory and secondary structure

The anti-cathepsin activity of bovine Lf hydrolysate samples was measured (Fig. 2) and the results are reported in Table 1. There was statistically no significant difference between the inhibitory efficacy of the samples H0 and H30 against any kind of cathepsins. This suggests that short-term hydrolysis and generation of the half molecules (Fig. 1a) did not affect the cathepsin inhibitory property of Lf. Prolongation of the hydrolysis process to 60 min and 90 min caused a significant increase in the cathepsin inhibitory property of Lf. When compared with H0, the CTSL IC_{50} of Lf decreased ~10.5 and ~92 folds due to hydrolysis for 60 min (H60), and 90 min (H90), respectively. H90 had a comparable inhibitory on CTSL and cathepsin B, but lesser inhibitory on two other cathepsins assessed in the present study (Table 1). Non-reducing SDS-PAGE indicated that the band corresponding to peptides with molecular masses of ~12 kDa became faint by hydrolysis ≥60 min (Fig. 1a). Nonetheless, it could not (completely) explain the increase in cathepsin inhibitory property of Lf by hydrolysis up to 90 min. Interestingly the Lf cathepsin inhibitory activity dramatically decreased by further prolonging the hydrolysis to ≥120 min. H120 and H0 had similar CTSL inhibitory, and H180 had even a lower CTSL inhibitory than H0. For other kinds of cathepsins, similar results were obtained by hydrolysis for ≥120 min. The cathepsin B and H inhibitory of H120 and H180 was lower than that of H0 and the inhibitory property of H120 and H180 on cathepsins K was not different from H0 (Table 1). For all types of cathepsins, the IC_{50} of the Lf hydrolysate was lowest at H90 and close to that of the synthetic cathepsin inhibitory compound, Z-Phe-Phe-fluoromethyl ketone (Table 1). The CTSL IC_{50} of the synthetic inhibitor was in the same order of magnitude (only 2.4 fold smaller) compared with H90.

In an attempt to explore the cause that explains the highest cathepsin inhibitory activity of H90 among all the hydrolysate samples, we assessed the secondary structure of Lf as influenced by hydrolysis was studied by FTIR spectroscopy. The amide I band (1600–1700 cm^{-1}) caused by C=O stretching (about 80%), coupled with in-phase N–H bending (Yang, Yang, Kong, Dong, & Yu, 2015) is primarily used for secondary structure studies. Therefore, the amide I band was derivatised and the structural features were determined. The allocation of the bands in the second-derivative amide I spectra to the structural features, i.e., unordered-helical structures (1646–1666 cm^{-1}), β-sheets, and β-turns was done according to Yang et al. (2015). It was not possible for us to separate the bands standing for unordered and helical (including α-helix) structures. Hence, a collective proportion of these two structures was determined.

Low α-helix content is a characteristic feature of many cysteine protease inhibitors such as bromelain inhibitor VI (Hatano, Kojima, Tanokura, & Takahashi, 1995), and the cytotoxic T-lymphocyte antigen-2β (Delaria et al., 1994). Indeed, Lf was employed in the present study because if its low α-helix content (Madadlou, 2020). Therefore, the percentile proportion of unordered-helical structures was measured and is reported in Table 1. The data indicate that H90 had the lowest content (i.e., percentile proportion) of unordered-helical structures amongst all the hydrolysate samples.

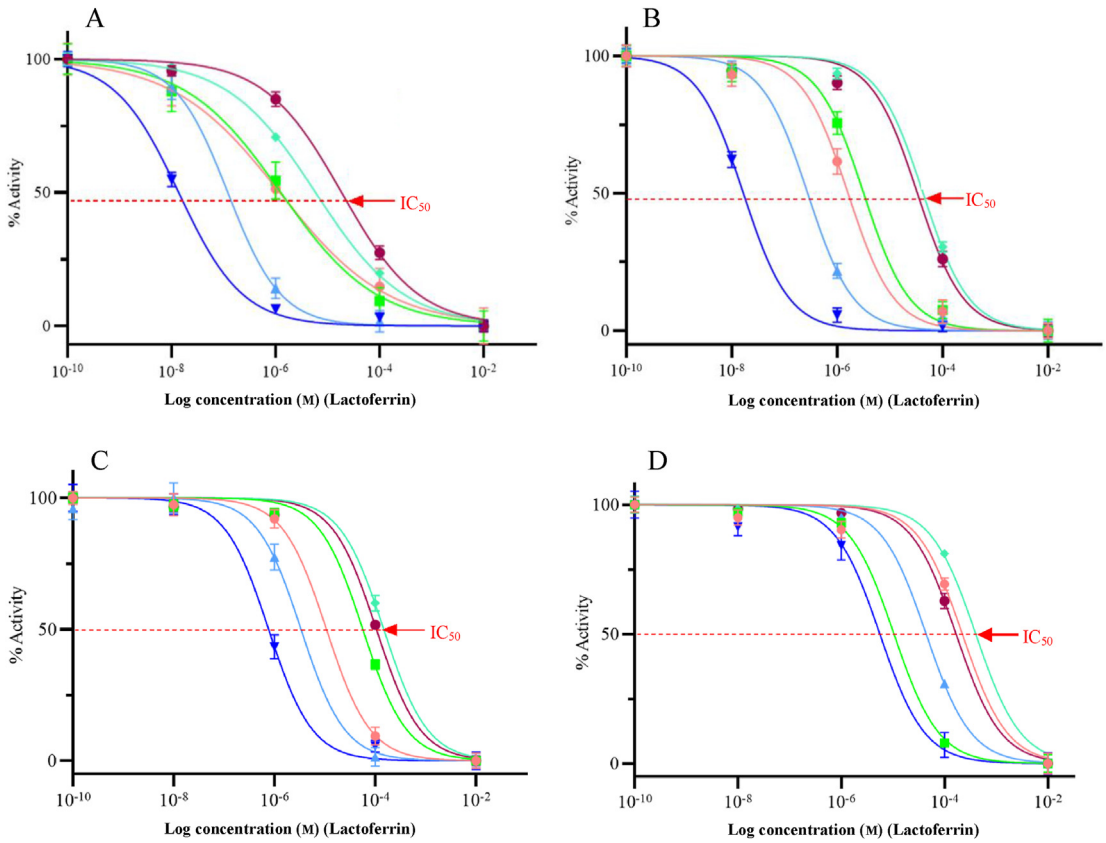

Fig. 2. Activity of human cathepsin enzymes (A, cathepsin L; B, cathepsin B; C, cathepsin H; D, cathepsin K) as affected by different concentrations of bovine lactoferrin hydrolysed for: ●, 0 min; ■, 30 min; ▲, 60 min; ▼, 90 min; ◆, 120 min; ●, 180 min.

Table 1
Cathepsin inhibitory, percentile proportion of unordered-helical secondary structures, and SARS-CoV-2 pseudovirus inhibitory of bovine lactoferrin hydrolysate.[a]

Sample	IC_{50} (M)				Unordered + helical structures (%)	IC_{50} (M) on pseudovirus
	Cathepsin L	Cathepsin B	Cathepsin H	Cathepsin K		
H0	$1.26 \times 10^{-6c,A}$	$1.61 \times 10^{-6c,A}$	$1.08 \times 10^{-5d,B}$	$2.21 \times 10^{-4d,C}$	44.93 ± 1.24	4.7×10^{-6c}
H30	$1.20 \times 10^{-6c,A}$	$3.20 \times 10^{-6c,A}$	$5.70 \times 10^{-5d,B}$	$1.05 \times 10^{-4d,C}$	43.90 ± 3.55	2.6×10^{-6b}
H60	$1.21 \times 10^{-7b,A}$	$2.77 \times 10^{-7b,A}$	$3.38 \times 10^{-6c,B}$	$4.42 \times 10^{-5c,C}$	43.84 ± 2.55	$2.8\ 10^{-6b}$
H90	$1.37 \times 10^{-8a,A}$	$1.67 \times 10^{-8a,A}$	$7.69 \times 10^{-7b,B}$	$5.61 \times 10^{-6b,C}$	41.74 ± 2.29	2.1×10^{-6a}
H120	$5.88 \times 10^{-6c,A}$	$4.29 \times 10^{-5d,B}$	$1.48 \times 10^{-4e,C}$	$4.03 \times 10^{-4d,C}$	49.24 ± 1.99	2.5×10^{-6b}
H180	$1.86 \times 10^{-5d,A}$	$3.34 \times 10^{-5d,A}$	$1.06 \times 10^{-4e,B}$	$1.68 \times 10^{-4d,B}$	47.79 ± 3.73	4.3×10^{-6c}
Reference inhibitor	5.70×10^{-9a}	8.14×10^{-9a}	6.30×10^{-9a}	9.50×10^{-9a}		

[a] H0—H180 indicate bovine lactoferrin hydrolysed for different times in min. The reference inhibitor, Z-Phe-Phe-fluoromethyl ketone, is a synthetic inhibitor of cathepsins used in the cathepsin inhibitory assay. IC_{50} is the concentration of bovine lactoferrin hydrolysate required to achieve 50% cathepsin inhibition; the IC_{50} on pseudovirus is the concentration of bovine lactoferrin that decreases a single round of infection by 50%. The determination of secondary structure was based on the second-derivative amide I FTIR spectra. Different lowercase superscript letters indicate significant differences ($p < 0.05$) in a column (in either the cathepsin inhibition assay or pseudovirus inhibition assay); different uppercase superscript letters indicate significant differences ($p < 0.05$) in a row, in the cathepsin inhibition assay.

Even though the percentile proportion of helical structures could not be individually determined, the data suggested an association between the highest cathepsin inhibitory and the lowest unordered-helical structures in H90. The data in Table 1 also indicated that extending the hydrolysis duration to ≥120 min increased the percentile proportion of unordered-helical structures. We assumed that some peptides which were generated by extended (≥120 min) hydrolysis aggregated and formed structures with higher helix contents. This assumption is supported with SDS-PAGE results. The most massive band identified under reducing SDS-PAGE, i.e., 15 kDa (Fig. 1b) became thicker when hydrolysis duration extended to 180 min. In agreement, other researchers have suggested an increase in α-helix content during protein/peptide aggregation (Ghosh et al., 2015). The increase in unordered-helical structures content due to extended hydrolysis coincided with low cathepsin inhibitory of H120 and H180 (Table 1).

3.3. SARS-CoV-2 pseudo-type infectivity assay

The efficacy of the bovine Lf hydrolysate samples in inhibition of SARS CoV-2 pseudo-type infectivity was assessed according to the method of (Hyseni et al., 2020) and the results are reported in Table 1. The IC_{50} value of the non-hydrolysed Lf (i.e., hydrolysed for 0 min, H0) and the Lf hydrolysed for the longest duration (H180) was approximately 4.5 μM. This disagrees with an earlier report where IC_{50} values less than 1 μM were reported for lactoferrin

against SARS-CoV-2 in various cell systems (Mirabelli et al., 2021). The disagreement is probably associated with the different methods used for the viral infectivity assessment in the present study and the referenced research (Mirabelli et al., 2021). Moreover, it is noteworthy that in the present study SARS-CoV-2 pseudotypes were used, whereas Mirabelli et al. (2021) used SARS-CoV-2.

The IC_{50} value against SARS-CoV-2 pseudo-types of the sample H90 was >2 fold smaller than that of H0 (Table 1), therefore the sample H90 showed a two times increased capacity to prevent the cell infection. The infectivity assay included entry of SARS-CoV-2 pseudo-types into target cells (HEK 293 T/17 cells) and involved the S protein engagement with the ACE2 receptor and priming of the S protein by TMPRSS2 (Hyseni et al., 2020). Although we could not employ a protocol to particularly study the role of CTSL in the pseudo-types entry to the target cells, the infectivity results are in accordance with CTSL inhibitory efficacy of the hydrolysate samples (Table 1).

The higher infectivity inhibitory of H90 compared with the other samples could be associated with its higher CTSL inhibitory, thus proving the relevance of the mechanism. However, the difference between the IC_{50} values of H0 and H90 against CTSL was approximately 90 times (see Table 1), which is enormously higher than the difference between the IC_{50} values of the samples against SARS-CoV-2 pseudovirus. This may indicate that the virus finds other ways to enter in the cells. In this respect, the inhibition of phosphatidylinositol 3-phosphate 5-kinase, TMPRSS2 or blocking two pore channel subtype 2 (Ou et al., 2020) together with CTSL inhibition might be more effective at preventing virus endocytosis. It is noteworthy that in the present study cathepsin inhibitory activity was measured using screening assay kits (abcam.com), not by cell cultures and hence, the CTSL inhibitory measured might not fairly indicate cathepsin inhibitory efficacy in cell studies.

4. Conclusion

Our data showed that hydrolysis by proteinase K can be used to modulate the cathepsin inhibitory of bovine Lf. The Lf sample hydrolysed for 90 min, i.e., H90 showed comparable CTSL and cathepsin B inhibitory and a lower inhibitory activity on cathepsins H and K. This is a positive feature as it may provide a venue for preferential inhibition of CTSL and cathepsin B by Lf without hazardously disturbing the functionality of other cathepsins. Such a preferential-selective inhibitory can be useful in treatment of diseases associated with over-expression of certain cathepsins.

A relationship was observed between the CTSL inhibitory and secondary structure of bovine Lf hydrolysates. A lower content of helical-unordered structures coincided with higher CTSL inhibitory. The literature supports a causative relationship between α-helix content and cathepsin inhibitory; however, as we could not individually and accurately measure the α-helix content in the present study, it remains to be explored whether the relationship is actually correlative (i.e., taking place concomitantly) or causative (i.e., lower helix structure causes higher cathepsin inhibitory).

In accordance with CTSL inhibitory, Lf hydrolysed for 90 min (H90) had a higher SARS-CoV-2 pseudovirus infectivity inhibitory than the Lf hydrolysed for either shorter (0, 30, 60 min) or longer (120, 180 min) durations. However, we noticed that hydrolysis for 90 min caused >90-fold reduction in the IC_{50} of Lf against CTSL, whereas it caused only a > 2-fold reduction in Lf IC_{50} against SARS-CoV-2 pseudovirus infectivity.

It is concluded that either inhibition of CTSL did not take place effectively in the pseudo-type virus experiments (when compared with CTLS inhibitor screening kit) or strategies other than (or together with) CTSL inhibition should be sought and developed for the infectivity inhibition.

Declaration of competing interest

None.

Acknowledgement

The authors are thankful to the Innovation Program Microbiology (IPM) of Wageningen University and Research (Wageningen, the Netherlands) for funding the project.

References

Baker, H. M., & Baker, E. N. (2004). Lactoferrin and iron: Structural and dynamic aspects of binding and release. *Biometals, 17*, 209–216.
Bokkhim, H., Tran, T., Bansal, N., Grøndahl, L., & Bhandari, B. (2014). Evaluation of different methods for determination of the iron saturation level in bovine lactoferrin. *Food Chemistry, 152*, 121–127.
Dana, D., & Pathak, S. K. (2020). A review of small molecule inhibitors and functional probes of human cathepsin L. *Molecules, 25*, Article 698.
Delaria, K., Fiorentino, L., Wallace, L., Tamburini, P., Brownell, E., & Muller, D. (1994). Inhibition of cathepsin L-like cysteine proteases by cytotoxic T-lymphocyte antigen-2 beta. *Journal of Biological Chemistry, 269*, 25172–25177.
Deng, J., Zhou, F., Heybati, K., Ali, S., Zuo, Q. K., Hou, W., et al. (2022). Efficacy of chloroquine and hydroxychloroquine for the treatment of hospitalized COVID-19 patients: A meta-analysis. *Future Virology, 17*, 95–118.
Fonović, M., & Turk, B. (2014). Cysteine cathepsins and extracellular matrix degradation. *Biochimica et Biophysica Acta (BBA) - General Subjects*, 2560–2570, 1840.
Ghosh, D., Singh, P. K., Sahay, S., Jha, N. N., Jacob, R. S., Sen, S., et al. (2015). Structure based aggregation studies reveal the presence of helix-rich intermediate during α-synuclein aggregation. *Scientific Reports, 5*, Article 9228.
Gomes, C. P., Fernandes, D. E., Casimiro, F., da Mata, G. F., Passos, M. T., Varela, P., et al. (2020). Cathepsin L in COVID-19: From pharmacological evidences to genetics. *Frontiers in Cellular and Infection Microbiology, 10*, Article 589505.
Goulding, D. A., O'Regan, J., Bovetto, L., O'Brien, N. M., & O'Mahony, J. A. (2021). Influence of thermal processing on the physicochemical properties of bovine lactoferrin. *International Dairy Journal, 119*, Article 105001.
Hatano, K. I., Kojima, M., Tanokura, M., & Takahashi, K. (1995). Primary structure, sequence-specific 1H-NMR Assignments and secondary structure in solution of bromelain inhibitor VI from pineapple stem. *European Journal of Biochemistry, 232*, 335–343.
Hernandez, A. V., Roman, Y. M., Pasupuleti, V., Barboza, J. J., & White, C. M. (2020). Hydroxychloroquine or chloroquine for treatment or prophylaxis of COVID-19. *Annals of Internal Medicine, 173*, 287–296.
Hoffmann, M., Kleine-Weber, H., Schroeder, S., Krüger, N., Herrler, T., Erichsen, S., et al. (2020). SARS-CoV-2 cell entry depends on ACE2 and TMPRSS2 and is blocked by a clinically proven protease inhibitor. *Cell, 181*, 271–280.
Hyseni, I., Molesti, E., Benincasa, L., Piu, P., Casa, E., Temperton, N. J., et al. (2020). Characterisation of SARS-CoV-2 lentiviral pseudotypes and correlation between pseudotype-based neutralisation assays and live virus-based micro neutralisation assays. *Viruses, 12*, Article 1011.
Lang, J., Yang, N., Deng, J., Liu, K., Yang, P., Zhang, G., et al. (2011). Inhibition of SARS pseudovirus cell entry by lactoferrin binding to heparan sulfate proteoglycans. *PLoS One, 6*, Article e23710.
Liu, C.-L., Guo, J., Zhang, X., Sukhova, G. K., Libby, P., & Shi, G.-P. (2018). Cysteine protease cathepsins in cardiovascular disease: From basic research to clinical trials. *Nature Reviews Cardiology, 15*, 351–370.
Liu, T., Luo, S., Libby, P., & Shi, G.-P. (2020). Cathepsin L-selective inhibitors: A potentially promising treatment for COVID-19 patients. *Pharmacology & Therapeutics, 213*, Article 107587.
Lönnerdal, B., Du, X., & Jiang, R. (2021). Biological activities of commercial bovine lactoferrin sources. *Biochemistry and Cell Biology, 99*, 35–46.
Madadlou, A. (2020). Food proteins are a potential resource for mining cathepsin L inhibitory drugs to combat SARS-CoV-2. *European Journal of Pharmacology, 885*, Article 173499.
Mirabelli, C., Wotring, J. W., Zhang, C. J., McCarty, S. M., Fursmidt, R., Pretto, C. D., et al. (2021). Morphological cell profiling of SARS-CoV-2 infection identifies drug repurposing candidates for COVID-19. *Proceedings of the National Academy of Sciences, 118*, Article 05815118.
Mittal, S., Mir, R. A., & Chauhan, S. S. (2011). Post-transcriptional regulation of human cathepsin L expression. *Biological Chemistry, 392*, Article 039.
Moore, S. A., Anderson, B. F., Groom, C. R., Haridas, M., & Baker, E. N. (1997). Three-dimensional structure of diferric bovine lactoferrin at 2.8 Å resolution. *Journal of Molecular Biology, 274*, 222–236.
Ohashi, A., Murata, E., Yamamoto, K., Majima, E., Sano, E., Le, Q., et al. (2003). New functions of lactoferrin and β-casein in mammalian milk as cysteine protease inhibitors. *Biochemical and Biophysical Research Communications, 306*, 98–103.
Ou, T., Mou, H., Zhang, L., Ojha, A., Choe, H., & Farzan, M. (2021). Hydroxychloroquine-mediated inhibition of SARS-CoV-2 entry is attenuated by TMPRSS2. *PLoS Pathogens, 17*, Article e1009212. h.

Ou, X., Liu, Y., Lei, X., Li, P., Mi, D., Ren, L., et al. (2020). Characterization of spike glycoprotein of SARS-CoV-2 on virus entry and its immune cross-reactivity with SARS-CoV. *Nature Communications, 11*, Article 1620.

Sano, E., Miyauchi, R., Takakura, N., Yamauchi, K., Murata, E., Le, Q. T., et al. (2005). Cysteine protease inhibitors in various milk preparations and its importance as a food. *Food Research International, 38*, 427–433.

Serrano, G., Kochergina, I., Albors, A., Diaz, E., Oroval, M., Hueso, G., et al. (2020). Liposomal lactoferrin as potential preventative and cure for COVID-19. *International Journal of Research in Health Sciences, 8*, 8–15.

Sharma, S., Singh, T. P., & Bhatia, K. L. (1999). Preparation and characterization of the N and C monoferric lobes of buffalo lactoferrin produced by proteolysis using proteinase K. *Journal of Dairy Research, 66*, 81–90.

Singh, J., Maurya, A., Singh, P. K., Viswanathan, V., Ahmad, M. I., Sharma, P., et al. (2021). A peptide bond from the inter-lobe segment in the bilobal lactoferrin Acts as a preferred site for cleavage for serine proteases to generate the perfect C-lobe: Structure of the pepsin hydrolyzed lactoferrin C-lobe at 2.28 Å resolution. *The Protein Journal, 40*, 857–866.

Singh, T. P., Sharma, S., Karthikeyan, S., Betzel, C., & Bhatia, K. L. (1998). Crystal structure of a complex formed between proteolytically-generated lactoferrin fragment and proteinase K. *Proteins: Structure, Function, and Genetics, 33*, 30–38.

V'kovski, P., Kratzel, A., Steiner, S., Stalder, H., & Thiel, V. (2021). Coronavirus biology and replication: Implications for SARS-CoV-2. *Nature Reviews Microbiology, 19*, 155–170.

Wotring, J. W., Fursmidt, R., Ward, L., & Sexton, J. Z. (2022). Evaluating the in vitro efficacy of bovine lactoferrin products against SARS-CoV-2 variants of concern. *Journal of Dairy Science, 105*, 2791–2802.

Xia, S., Liu, M., Wang, C., Xu, W., Lan, Q., Feng, S., et al. (2020). Inhibition of SARS-CoV-2 (previously 2019-nCoV) infection by a highly potent pan-coronavirus fusion inhibitor targeting its spike protein that harbors a high capacity to mediate membrane fusion. *Cell Research, 30*, 343–355.

Yang, H., Yang, S., Kong, J., Dong, A., & Yu, S. (2015). Obtaining information about protein secondary structures in aqueous solution using Fourier transform IR spectroscopy. *Nature Protocols, 10*, 382–396.

Zhao, M.-M., Yang, W.-L., Yang, F.-Y., Zhang, L., Huang, W.-J., Hou, W., et al. (2021). Cathepsin L plays a key role in SARS-CoV-2 infection in humans and humanized mice and is a promising target for new drug development. *Signal Transduction and Targeted Therapy, 6*, Article 134.